Two complimentary codes in the superior colliculus differentiate external from self-generated tactile cues

Suma Chinta and Scott R. Pluta, Department of Biology, Purdue University, West Lafayette, IN

Abstract

Perception is often the expected outcome of our actions, while at other times it emerges from unexpected changes in the scene. During spatial navigation, animals must differentiate between cues generated by self-motion from motion that originated externally. To reveal the neural basis of this perceptual ability, we examined the midbrain superior colliculus (SC), which contains an egocentric map of sensorimotor space. By simulating whisker-guided navigation through a dynamic landscape, we discovered a transient neural response that selectively emerged for unexpected, externally generated tactile motion. This transient response only emerged when external motion engaged different whiskers, arguing that sensorimotor predictions are specific to a somatotopic location. When external motion engaged the same whiskers, neurons encoded surface motion with shifts in spike timing correlated to self-generated tactile features. Thus, a persistent representation of self-generated touch may be necessary to encode spatial features finer than the receptor array. In conclusion, the SC contains complementary rate and temporal codes to differentiate external from self-generated spatial features during tactile localization.

Introduction

Navigation is an active process involving the integration of self-generated spatial cues. For example, humans move their eyes to scan a scene or stroke a surface to identify its contour. To move through space, animals must differentiate the expected consequences of their actions from unexpected external motion. What are the neural mechanisms underlying this fundamental perceptual ability?

To answer this question, we focused on the midbrain superior colliculus (SC), which contains multiple egocentric maps of sensorimotor space[1–4]. Many SC mediated behaviors involve spatial navigation, such as pursuing prey and escaping predators. While tracking a target with the eyes, the SC appears vital for stabilizing the visual field and correcting movement errors. Given these insights, we sought to uncover how SC neurons differentially encode external and self-generated spatial cues. Since the SC is also important for sustaining fixation on stationary targets, we expected to find a complementary code supporting spatial localization for periods of external stability.

While decades of research have outlined SC function during visuospatial processing, surprisingly less is known in the context of somatosensation[5–7]. The mouse SC is known to encode whisker stimuli, yet nearly all published work in this area has been performed under anesthesia[4,8–11]. These experiments revealed that the SC contains a somatotopic map of whisker space, whereby individual neurons possess large receptive fields that are sensitive to whisker motion. The characterization of sensory responses in the SC has occurred primarily during visual fixation. While this approach has been invaluable for segregating sensory and motor activity, it cannot reveal the neural mechanisms for distinguishing external from self-generated spatial cues. The somatosensory whisker system of mice offers a powerful model for investigating this question.

To determine active somatosensory features encoded by SC neurons, we designed an experiment that mimics whisker-guided navigation. While running on a treadmill, mice rhythmically touched a cylindrical surface that rotated at the same velocity as their locomotion. This created a tactile flow-field that simulates running along a wall, in a manner similar to visual flow. Periodically, the flow-field translated along the mouse's horizontal axis, effectively changing the surface contour against the whiskers. Using spike times from large populations of SC neurons, we accurately decoded surface movements, with greatest accuracy for locations that engaged different whiskers. We identified a transient response in SC neurons that selectively emerged during unexpected, externally generated changes in tactile space. A persistent code based primarily on spike timing was also observed that appears specialized for encoding self-generated tactile features.

Results

Whisker-guided virtual navigation

To determine the neural mechanisms underlying active, tactile localization in the superior colliculus (SC), we designed an experiment that mimics navigation (Fig. 1A). To simulate tactile navigation along a wall or narrow corridor, a head-fixed mouse was placed on a treadmill whose locomotion speed controlled the rotation of a nearby cylindrical surface. Locomoting mice rhythmically touched the surface with their whiskers while a high-speed (500fps) infrared camera and digital encoders recorded whisker kinematics, surface location, and running speed (Fig. 1C). To obscure visual and auditory cues, an opaque flag blocked visual cues and white noise was broadcasted. During a given trial, the cylindrical surface translated rostral or caudal or remained at the center/home position. After staying at the new location for a set locomotor distance, the surface would return to the home position. While running, mice adapted the position of their whiskers to track surface translations. (Fig. 1B). Since translations were triggered by locomotor distance, variation in locomotion speed made translation onset difficult to predict (Fig. 1C). A 3-shank, 128-channel silicon probe recorded neural activity simultaneously across the intermediate and deep layers of the lateral SC, approximately 300 – 1000 microns below its surface (Fig. 1D, 12 mice, 873 neurons). More than half of all SC neurons displayed a significant response to surface translation (67 ± 6%, 12 mice, 578 neurons, $p < 0.05$, 1-way ANOVA).

The superior colliculus performs tactile localization with transient and persistent changes in firing rate

SC neurons responded to surface translations with distinct changes in firing rate that enabled accurate decoding of surface location. With the surface in the home location, baseline firing rates among neurons were mixed, ranging from less than one to more than 50 per second. During surface translations into rostral or caudal space (Fig. 2A), the firing rate of most neurons rapidly increased while other neurons decreased, as shown in three example units (Fig. 2B). Interestingly, neural responses had two distinct response components based on their rate of adaptation. We refer to these tactile response components as 'transient' (a short rapidly adapting response) or 'persistent' (sustained change in spike rate often following a transient). We classified neurons as transient or persistent neurons based on their rate and magnitude of adaptation (Fig. 2C). To understand the information content among these neuron types, we tested the localization accuracy of population-level SC activity over time. Using an SVM classifier, we discovered that SC activity accurately predicted surface location, with the highest

performance around the translation period, as shown in one example mouse (Fig. 2D, 99% accuracy, 76 total neurons). Classification accuracy for persistent neurons was accurate throughout the entire trial, in line with their sustained changes in firing rate (30 neurons, 1 mouse). On the other hand, transient neurons performed accurately only during the initial period of external motion, as expected due to their rapid adaptation rates (46 neurons, 1 mouse). This general trend was consistent across our population of mice, despite some heterogeneity in overall classifier performance (Fig. 2E, 68.2 ± 5.2% accuracy, 12 mice, 475 neurons). To complement our statistical classifier, we calculated location modulation indices (Suppl. Fig. 1A,B), and found that neural populations displaying the largest response differences between rostral and caudal locations also had the highest classification accuracies (Suppl. Fig. 1C). Transient and persistent components were somatosensory in origin, since spikes were precisely timed relative to the onset of whisker protraction in both the transient and persistent trial periods (Fig. 2F).

Gains and losses in whisker contact drive accurate neural representations of surface location

To reveal the stimulus variables driving SC responses, we examined the dynamics of whisker touch during surface translation. We discovered that surface translation elicited large changes in firing rate only when whiskers gained (GoW) or lost (LoW) contact with the surface (Fig. 3A). The addition or subtraction of a single whisker from the surface was sufficient for this effect. Most neurons preferentially responded to whisker addition (GoW, 52 ± 1%, 6 mice, 336 neurons, Fig. 3B), while only a small percentage of neurons preferred surface translations that engaged the same whiskers at both locations (15 ± 3%, 6 mice, 336 neurons). Accordingly, neural decoding of surface location was much higher during translations that engaged different whiskers (GoW & LoW, 8 mice), relative to translations that sustained touch with the same whiskers (4 mice, Fig. 3C). In two mice, we repeated the experiment after trimming the whiskers and found that nearly all neurons lost their responsiveness to surface translation (59 ± 4% pre-trimming vs. 6 ± 1% post-trimming, $n = 156$, paired t-test, $p < 0.05$, Fig. 3D), demonstrating the necessity of touch to encode changes in surface location.

To understand response diversity in the framework of whisker space, we quantified each neuron's response to GoW and LoW separately (10 mice, 529 neurons, Fig. 3E). Almost half of all neurons increased their firing rate during both GoW and LoW (251/529 neurons), while the remaining neurons increased their firing rate for one stimulus type yet decreased it for the other. To illustrate these effects, we plotted the population averaged firing rates of each response type relative to the onset of surface translation (Fig. 3F). Overall, these data demonstrate that SC neurons were sensitive to changes in whisker contacts, while showing relatively weak changes in firing rate during translations that maintain contact with the same whiskers (Fig. 3G).

The transient response selectively emerged during externally generated changes in whisker contact

We hypothesized that the large, transient response was caused by externally generated changes in whisker contact. To test this hypothesis, we modified our experiment so that the surface stayed either in rostral space or entirely outside the whisking field for an extended period (Fig 4A). Occasionally the surface translated from outside the whisking field to the rostral space causing an externally generated tactile response (external GoW). With the surface in rostral space, mice voluntarily lost and gained touch (Self LoW/GoW) with the surface as they

periodically (7.2 ± 5.6 second interval) transitioned between resting (no running or touch) and locomotive whisking (Fig. 4B). Importantly, this self-imposed interval between losses and gains in whisker contact was similar to the interval between externally generated changes in whisker contact. When surface translation contacted whiskers, many neurons displayed a large transient response (Fig. 4C,D). However, when the mouse voluntarily touched the surface, the transient response never emerged (Fig. 4E, $p=8e^{-05}$, 41 neurons with transient, 2 mice), and neuronal firing rates stayed constant, reflecting the persistent dynamics of self-generated touch (Fig. 4F, p=0.26, 121 neurons, 2 mice).

The transient response encodes stimulus novelty

Next, we sought to determine if responses to externally generated whisker change were static or modulated by higher-level stimulus features. We analyzed the effect of GoW repetition on the magnitude of multiple response components (Fig 3B). For each experiment, we selected a GoW stimulus and calculated the baseline (BR), transient (TR), and persistent (PR) response components a function of repetition, as shown in one example neuron (Fig 5A). Importantly, these GoW stimuli were interleaved with other stimulus translations due to the random trial structure (Fig 1C). We discovered that TR magnitude decayed with increasing GoW repetitions while the PR and BR components remained stable. This TR-specific habituation was consistent across the population (Fig. 5B, 148 neurons, 10 mice, $p = 5.5e^{-5}$ for TR; p = 0.24 for SR; p = 0.74 for BR, t-test), and was unlikely caused by receptor-level adaptation, since the average interval between each GoW event was greater than one minute (67 ± 5 sec, 10 mice).

To examine the representation of stimulus novelty within simultaneously recorded populations of neurons, we decoded stimulus repetition using all transient responsive neurons in individual mice (28 ± 8 neurons per mouse). Using a linear regression model with 5-fold cross-validation, the TR component accurately predicted repetition number in seven of ten mice, while BR and PR components predicted repetition in only one mouse each (Fig. 5D,E, variance explained is 45 ± 6% for TR, 0.73 ± 10% for PR, -17 ± 9% for BR, 7 mice). Interestingly, TR habituation may also be controlled by stimulus probability, as the rate of habituation was significantly higher for GoW translations with 100% probability (surface return from rostral), when compared to GoW translations in the same mice with 33% probability (surface excursion from center) (Fig. 5C 32 TR neurons in 2 mice, p = 0.0026, signed rank). Therefore, sensory expectation appears to control the rate of SC habituation.

Spike timing is correlated with the rhythm of self-generated tactile features

Since surface translations engaging the same whiskers caused only modest change in overall firing rate, we speculated there might be a shift in temporal pattern of spikes that support localization. To test this hypothesis, we first assessed the presence of any temporal pattern of spiking by aligning spike rasters to the start of whisker protraction (Fig. 6A,C). Neurons displayed non-uniform spike profiles demonstrating the presence of a temporal code beneath the rate code. To align spikes to specific periods of whisking, we created spike-triggered averages of whisker phase (STAs or phase tuning, Fig. 6B, D, see methods). A large fraction of neurons displayed phase tuning distributions that were significantly different from chance, during both free whisking in air and against the surface (31 ± 4% free whisking, 6 mice, 154 neurons; 45 ± 4% surface whisking, 12 mice, 378 neurons).

Next, we observed that the increases in whisker curvature that occurred during protraction and the decreases that occurred during retraction were correlated with the phase tuning of neurons (Fig. 6 B, D). In some neurons, we observed a striking resemblance between their phase-tuning distribution and whisker curvature-phase distribution (Fig. 6E). To examine this relationship, we calculated the maximum correlation coefficient between the neuronal phase tuning and the phase-shifted whisker curvature, allowing us to adjust for any arbitrary differences in spike latency. The majority (213/378, 56%) of phase tuning curves were strongly ($R > 0.7$) correlated (bend facilitated) or strongly anti-correlated (bend suppressed) with whisker curvature (Fig. 6F). Across the population, neurons primarily preferred phase angles shortly after the start of protraction or retraction (Fig. 6G), demonstrating a preference for either an increase or a decrease in curvature at the rapid timescale of a single whisk cycle.

Shifts in spike timing encode surface translations that engage the same whiskers

Surface location has a profound effect on whisker curvature. We reasoned that if the profile of whisker curvature controls spike timing, then the phase tuning of neurons should shift in accordance with changes in its shape. When the surface translated caudally, the curvature profile broadened, and its peak shifted slightly towards the start of protraction (Fig. 7A). This broadening of the profile correlated with a decrease (broadening) in phase selectivity, as shown in the four example units. To illustrate this effect across the population, we compared phase tuning between two surface locations. In the more caudal location, neuronal phase selectivity significantly decreased ($p = 1e^{-7}$, paired-sample t test) while phase preference shifted towards the start of protraction ($p = 5.6e^{-3}$, paired-sample t test, Fig. 7B,C), demonstrating significant changes in spike timing. Locomotion speed between surface locations was nearly identical, indicating that changes in run speed was not the primary cause of this effect (Suppl. Fig. 2). Therefore, temporal spike dependence of SC neurons on the curvature profile of whiskers enables localization of surface translation that engage the same whiskers.

Discussion

Navigation is a natural behavior that contextualizes incoming sensory stimuli with outgoing motor commands. To perform this feat, an internal model of self-motion is essential to recognize if changes in egocentric space originate from externally or internally generated movements[12,13]. By simulating whisker-guided navigation, we discovered that the mouse SC is specialized for locating unexpected, externally generated changes in tactile space. We identified a transient response (TR) component, found in many SC neurons, which selectively emerges during externally initiated touch and habituates in a context-specific manner. Habituation of the TR occurred independently of persistent tactile responses, providing evidence for multiple distinct circuits controlling SC activity.

Both the barrel cortex and brainstem provide monosynaptic tactile sensory drive to SC neurons[8–10,14,15]. How SC neurons balance these inputs with higher-order motor and associative signals to contextualize stimulus information remains an important topic. We hypothesize that an efference copy of whisker motion, possibly involving the cerebellum, motor cortex and brainstem, is critical for SC neurons to distinguish external from internally generated changes in tactile space[16–21]. Value-coded output from the basal ganglia could further shape the transient response in SC neurons to generate a neural mechanism for orienting towards novel or

rewarding environmental cues[22–28]. Importantly, mice in our study were behaved voluntarily, not seeking reward. In this free-form context, habituation of the TR may reflect a central mechanism for ignoring stimuli of diminishing value[29]. In different behavioral contexts, goal-directed processing may flexibly control the TR to match the expected value of the target stimulus[30–33]. Additional work is needed to determine whether the TR responses described here encode value of environmental cues while decision making. Habituation of visual responses has been observed previously in primates and rodents[34–37]. Our study is the first to show tactile stimulus habituation in the SC supporting sensory expectations.

Population decoding of surface location was accurate only when its movement engaged different whiskers. This argues that a somatotopic map of whisker space is central to object localization in the SC. Given this result, one might assume that SC neurons can only encode coarse, whisker-level changes in space. However, we found that shifts in spike timing relative to whisker phase encode object movements that engage the same whiskers. The foundation for this claim is the strong correlation between neuronal phase tuning and the temporal profile of whisker curvature. As the surface moved caudal, the profile of curvature broadened and shifted forward, leading to equivalent changes in spike timing. The circuit mechanisms underlying SC phase tuning are unknown, but inputs from both the brainstem and barrel cortex are candidates[38–41]. These somatosensory inputs to the SC spike primarily during periods of protraction, yet we discovered that many SC neurons prefer the opposite phase (retraction). Therefore, the SC may perform a local computation (bend suppression) that enhances spike probability for periods opposite its inputs. Pathway specific perturbation experiments could provide further insights into which sensory upstream regions contribute to the phase coding of surface location. While shifts in phase tuning may encode relative differences in surface location, an internal model of whisker position is necessary for decoding absolute distance in egocentric space[42,43]. Nonetheless, our results establish spike timing as a potential mechanism for obtaining hyperacuity using an active sensor array[44].

Experimental Methods

Experimental Model and Subject Details

Mice of a CD-1 background of both sexes, between the ages of 9-15 weeks were used for all experiments. The Purdue Institutional Animal Care and Use Committee (IACUC) and the Laboratory Animal Program (LAP) approved all procedures. Mice were socially house with five or less per cage and maintained in reverse light-dark cycle (12:12 hr.). All experiments were conducted during the animal's subjective night.

Method Details

In-vivo Electrophysiology

Prior to behavioral conditioning, a custom stainless steel headplate was attached to each mouse to enable head fixation. Briefly, animals were anesthetized under 5% isoflurane and maintained at ~3% while monitoring body temperature and respiratory rate throughout the procedure. Artificial tears ointment was applied to keep the eyes hydrated. The skin and fur over the skull were disinfected with 70% ethanol followed by betadine and incised using sterilized surgical instruments. A tissue adhesive (Liquivet) and dental cement (Metabond) was applied over the skull and wound margins. The headplate was attached to the skull with dental cement. Lastly buprenorphine (mg/kg) was administered as a postoperative analgesic. Two days after headplate implantation, mice were placed on a circular treadmill for 1 hour per day for up to 10 days, or until they learned to run freely at a steady pace.

On the day of the electrophysiology recording, mice were briefly anesthetized to perform a craniotomy over the SC. A 1mm diameter craniotomy was made using a biopsy punch (Robbins

Instruments) and then covered with a silicone gel (Dowsil). After 2-3 hours of recovery, mice were placed in the experimental rig and a three-shank custom probe (Neuronexus) of 128-channels was lowered into the brain using a micromanipulator (NewScale). After exiting the ventral surface of the cortex, as evident by a loss of spiking, the electrode was lowered at a rate of 75µm/min while constantly searching for activity driven by flashes of light. The onset of visual activity was used to mark the depth of the SC surface (~1000µm below cortical surface). The electrode was further lowered into the intermediate and deep layers, where manual whisker deflections caused strong neuronal responses. The receptive field of neurons were mapped by manually deflecting individual whiskers and locating the primary drivers of neuronal activity. Whiskers that did not elicit detectable activity were trimmed for ease during whisker labeling. Recordings were targeted towards the C-row and macrovibrissae. If the electrode penetration missed the target, it was removed and re-inserted based on the coordinates of somatotopic space. In most experiments, mice had 3 – 5 intact whiskers contacting the surface, which spanned one or two rows. In other cases, mice had two whiskers intact.

Whisker guided virtual navigation

The circular treadmill was attached to a digital encoder that drove the rotation of a tactile surface in a closed-loop. A trial began after 200cm of locomotion on the treadmill to ensure the mouse was actively sensing the surface. Shortly (1.4 sec.) after the trial began, the surface either translated 1 cm linear distance into rostral or caudal space or remained at the center/home location. Each outcome was randomly chosen with equal (33.33%) probability. In six mice, an additional location was added that was entirely outside the whisker field, giving each excursion a random 25% probability. While at the rostral/caudal position, mice had to run an additional 200cm before the surface would return to the center. An opaque flag over the eye and white background noise obscured visual and auditory cues, respectively.

We modified the translations for two mice to record responses during self- and external-GoW. The surface translated between two locations: rostral or entirely outside the whisking field. The average interval between translations was 20.3 ± 3 seconds, while the average interval between two successive translations resulting in external-GoW was 74.6 ± 0.6 seconds. The standard deviation of the interval between translations was 12.8 seconds, due to variation in mouse locomotion speed. External-GoW occurred when the surface translated into the whisking field while the mouse was locomoting. Self-motion occurred when the surface was outside the whisking field, and mice transitioned from resting to locomotive whisking in air periodically. Self-GoW occurred when the surface was stationary in the whisking field, allowing periodic bouts of self-motion to induce surface whisking.

Whisker Tracking & kinematics

Whiskers were tracked at 500fps during the trial. A high-speed infrared camera (Photonfocus DR1) and a mirror angled at 45 degrees captured whisker motion under IR illumination. Videos were synchronized with neural data via external triggers generated by a National Instruments card and recorded on an Intan 512 controller. DeepLabCut was used to label the whisker(s) and track their movement[45]. Four evenly spaced points on each whisker were labeled. Approximately 150 frames were manually labeled from each experiment spanning all surface positions. The DLC neural network was trained for at least 200k iterations and the final labels were manually checked for accuracy. Whisker position/angle was calculated for each label on each whisker with reference to a user defined point on the face relative to the frame's vertical axis. Whisker bend/curvature was calculated from the three distal labels on each whisker using Menger curvature. The whisker bend derivative was calculated as the local slope with cubic approximation in a moving window of 100ms. Whisker angle was bandpass filtered (1-30Hz, fdesign.bandpass order 4, MATLAB), Hilbert transformed (hilbert, MATLAB), and the phase

angle was obtained from the complex value (angle, MATLAB). A phase angle of zero depicts the most protracted angle, while +/- π was the most retracted angle.

Spike Sorting

Spikes sorting was performed using the Kilosort2[46] and manually curated using Phy2 gui (https://github.com/cortex-lab/phy). Spike clusters were considered single units based on their spike waveform, location on the electrode, and cross-correlogram of spike times. Single units were used for all analyses in the paper.

Statistical Analysis

Location classifier

To classify the location of the tactile surface from population-level SC activity, we applied the Neural Decoding Toolbox[47] using a support vector machine (SVM). The classifier predicted surface location (rostral, caudal, center) throughout the duration of the trial. Only responsive neurons for surface translation were used. Spike data was first Z-scored to prevent high firing rate neurons from having a disproportionate influence on classification. The spike rate of every neuron was calculated using 150ms bins and surface location was predicted every 20ms to plot classification accuracies over time. A 10-fold cross validation was performed along with 50 resample runs to calculate a robust estimate of classification accuracies. The classification accuracy was measured based on the zero-one loss function.

Modulation Indices

All modulation indices (RMI, CMI, GoW, LoW) were calculated as the difference divided by the sum of spike rate averages in a 500 ms bin during the translation and the baseline period. To measure the discriminability between rostral and caudal translations, we measured the distance value (d-value) which is the distance of a point from the line of unity on the RMI CMI plot.

Transient (TR), Persistent (PR), and Baseline (BR) response components:

A translation was defined as a GoW/LoW when at least one whisker gained or lost contact with the surface. Trials with sustained touch maintained contact with the same whiskers during surface translation. Since changes in whisker space (GoW/LoW) happened at slight time differences across mice, we selected a custom window for the TR for each mouse based on the population average firing rate for every whisker change translation. We verified this window onset with kinematic analysis of high-speed videos. The PR was calculated 1.0 – 1.4 seconds after the start of translation, while BR was calculated in the 400ms window before the start of translation. We performed a one-way ANOVA (MATLAB function anova1) on the BR, TR, and the PR windows for every neuron. A Tukey post hoc test (multcompare, MATLAB) was used to test for significant ($\alpha < 0.05$) differences between the BR, TR, and PR. Neurons with significantly different TR and/or PR from BR were called tactile responsive neurons and used for all analyses. TR neurons had a mean firing rate during the initial responsw window that was significantly greater than the BR and PR.

Stimulus repetition

To obtain repetition slopes, we fit firing rates of TR neurons in the TR, PR and BR window with a linear regression model using the MATLAB fitlm function. Only neurons with a significant linear fit were included in the population analysis.

To decode repetition number, we used all TR neurons that did not drift. Neuronal drift was determined by testing if the spontaneous firing rate during the first 10 trials was different from the last 10 trials using a Wilcoxon signed rank test. The firing rate of the selected neurons within

the TR, PR, and BR windows was then used to predict the repetition number using the SVM regression (fitrsvm, MATLAB) with 5-fold cross validation where the model is trained and tested on different data sets. Prediction accuracy was reported as percent variance explained. In the below equation, R^2 is the fraction of variance explained, $\hat{y}_i$ are the predicted values, y_i are the true values, and $\bar{y}$ is the mean value of $true\ values$.

$$R^2 = 1 - \frac{\sum_i(\hat{y}_i - y_i)^2}{\sum_i(y_i - \bar{y})^2}$$

Self-GoW and external-GoW

Self-GoW and external-GoW was calculated in the transient and the persistent window. Self-GoW was calculated as a difference between mean firing rates of self-GoW and self-motion. External-GoW was calculated during surface translation as the difference between the mean firing rates during the TR/PR and baseline window.

Phase tuning

To obtain each neuronal phase tuning curves, we generated spike triggered averages of whisker phase (STA). Spike counts for each neuron were binned into 20^0 non-overlapping phase bins spanning from – π to +π, determined by the phase angle at the time of each spike. To calculate firing rate, spike counts in each phase bin was divided by time the whiskers spent at each angle. Neurons were considered phase tuned if their firing rate distribution of phase (STA) was significantly different from a chance distribution (χ^2 goodness of fit, $\alpha < .05$). The phase preference of each neuron was the circular mean of its phase tuning curve[48], while the phase selectivity was the modulation depth, which was the difference divided by the sum of maximum and minimum STA firing rates.

Figures

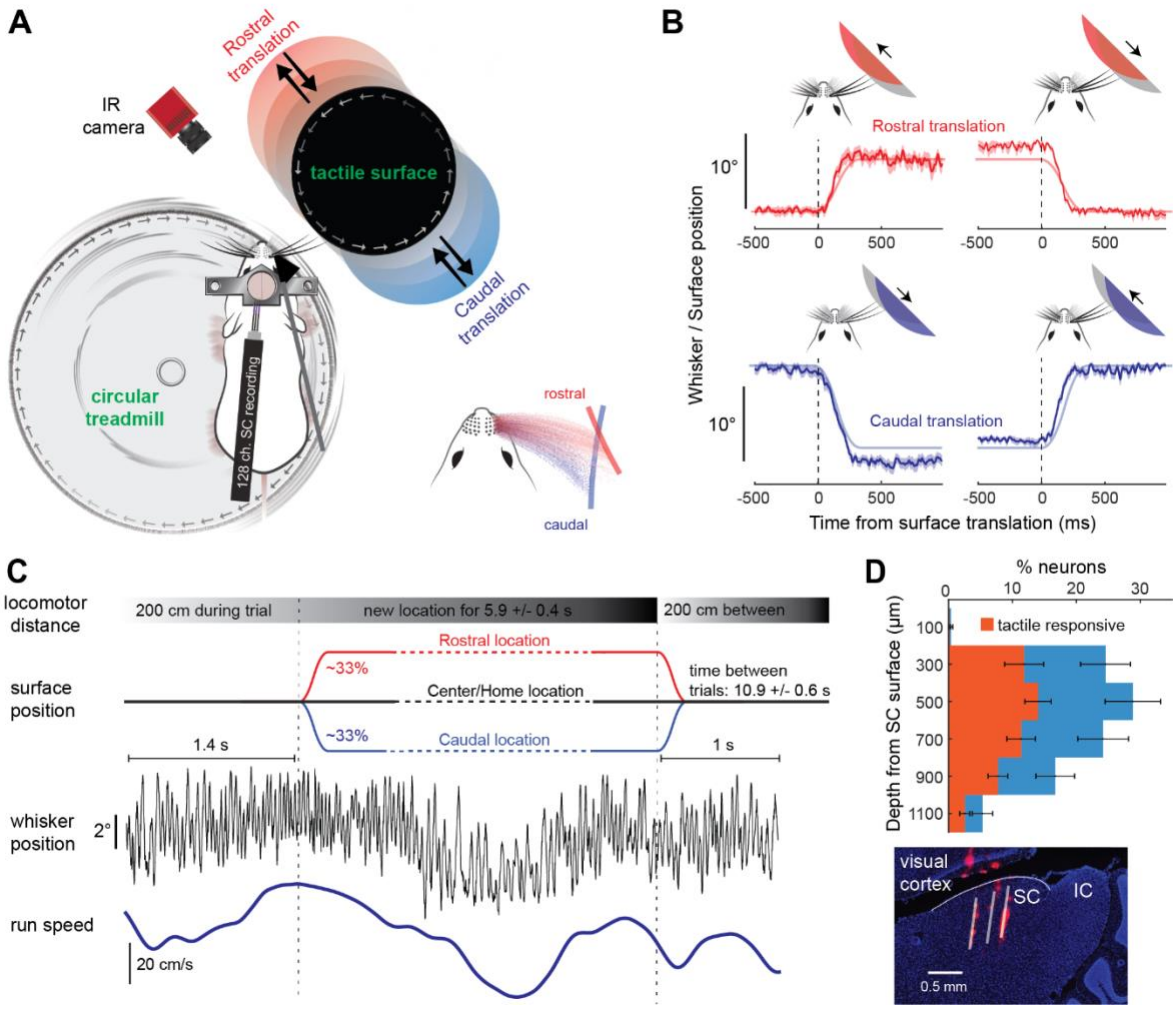

Figure 1. Tactile dynamics during whisker guided virtual navigation
A) Schematic of whisker guided virtual navigation, illustrating a head-fixed mouse locomoting on a treadmill and whisking against a surface. After trial initiation, there was an equal probability for the tactile surface to translate into either rostral (in red) or caudal (in blue) whisker space or staying at the center position (in black). Bottom right: single-whisker location density while the surface was at the rostral or caudal location. B) Whisker position (mean ± s.e.m) and surface location (transparent line) during rostral (top in red) and caudal (bottom in blue) translations. The first half is surface excursion while second half is the return to the center position. C) Trial structure aligning surface position, whisker position, and locomotion speed. D) Top: Percentage of tactile responsive SC neurons (orange) and total recorded neurons (blue) at various depths from the SC surface (12 mice, 873 neurons). Bottom: dye tracing of the electrode shanks in the intermediate and deep layers of the lateral SC.

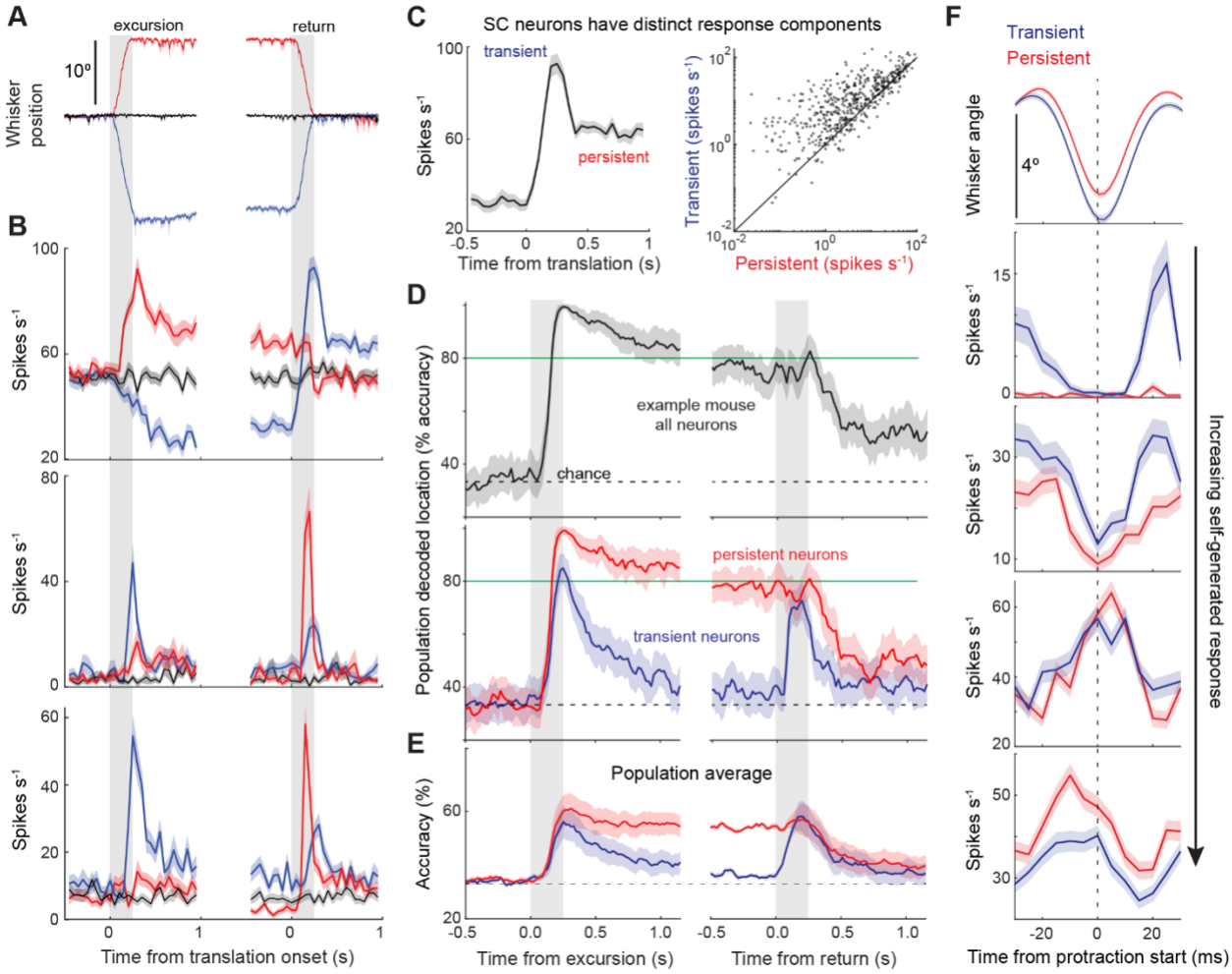

Figure 2. Superior colliculus accurately encodes surface translation across multiple timescales A) Top: Trial averaged whisker position during rostral (red), center (black) and caudal (blue) translations in an example experiment. B) Histograms of firing rates for three example neurons in the same experiment. Grey shaded regions represent the surface translation periods. C) Left, an example neuron illustrating the distinct transient and persistent response components evoked during surface translation. Right, scatter plot comparing the transient and persistent firing rates of neurons (10 mice, 529 neurons). D) Top, neural decoding of surface location over time using all of the neurons recorded from one experiment (76 neurons, black trace). Bottom, same as above but using only the persistent neurons (30 neurons, red) or only the transient neurons (46 neurons, blue). The black dashed line indicates the chance decoder performance of 1/3rd correct. E) Population averaged neural decoding for all persistent and transient neurons (12 mice). F) Top, whisker angle aligned to the start of protraction. Bottom, firing rates of four example neurons aligned to the start of whisker protraction. Firing rates were plotted separately for the transient (blue) and persistent (red) response periods. All values are mean ± s.e.m.

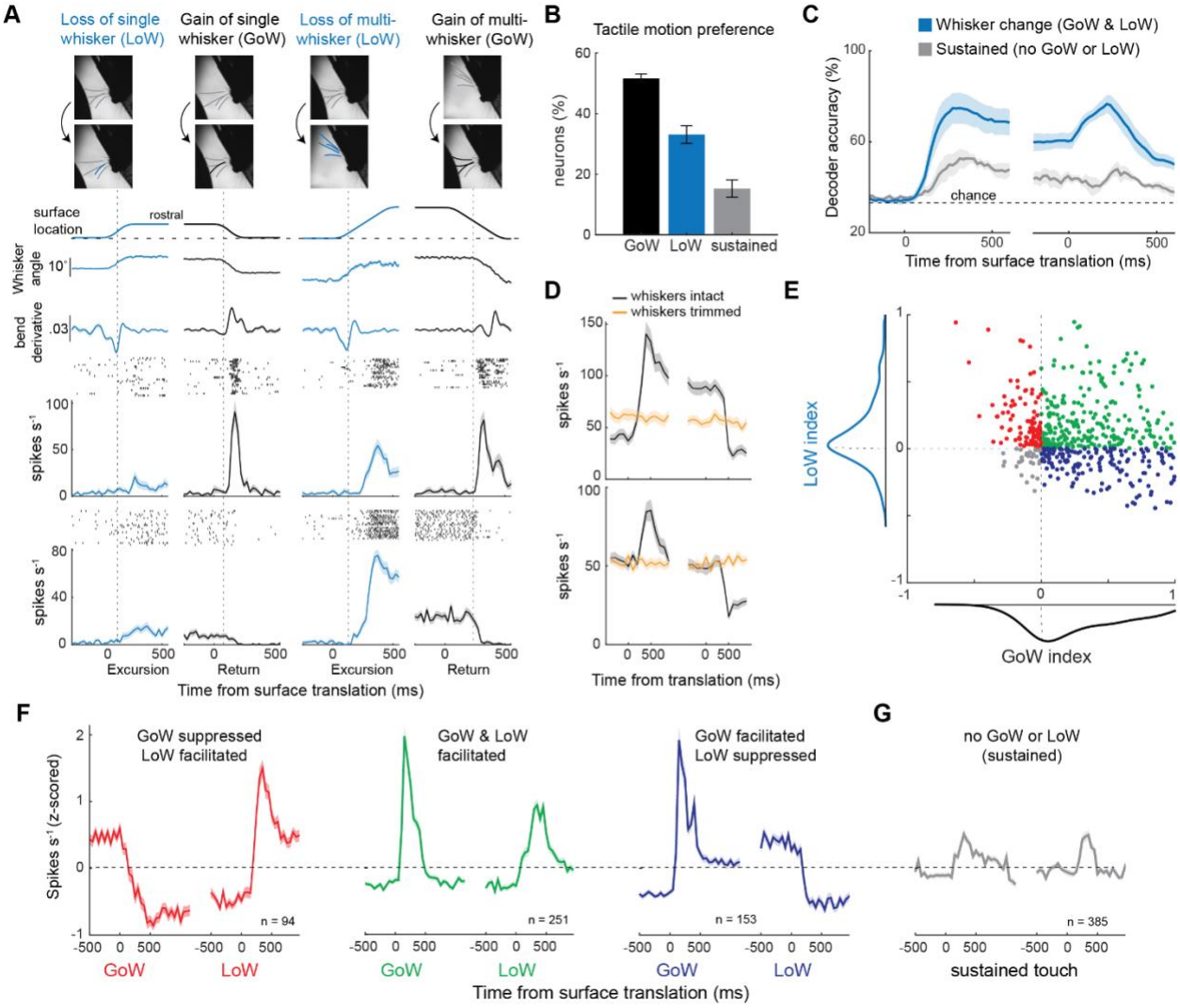

Figure 3. Gains and losses in whisker touch drive transient and persistent changes in spike rate A) Surface location, whisker angle, whisker bend derivative, and the firing rates of two example neurons during gains (black) and losses (blue) in whisker touch. Dashed line marks the estimated moment of whisker change, based on whisker kinematics. The two bottom rows are example neurons, and each column is a unique change in whisker space indicated at the top. B) Percentage of neurons that preferred a gain of whisker contact (GoW, 52 ± 1%), loss of whisker contact (LoW, 33 ± 3%), or sustained touch (15 ± 3%, 6 mice, 336 neurons). C) Neural decoding of surface location for translations that contacted different whiskers (blue, 8 mice) vs translations that maintained contact with same whiskers (black, 4 mice). Dashed line is chance accuracy of 33%. D) The firing rate of two example neurons during whisker change with intact whiskers and after all the whiskers were trimmed off. E) Scatter plot comparing the normalized GoW and LoW responses of each neuron (10 mice, 529 neurons). F) Population averaged, z-scored firing rates of neurons grouped by the sign (> zero or < zero) of their response to GoW and LoW. G) Population averaged, z-scored firing rates of neurons during translations that maintain contact with the same whiskers (excursion and return, 8 mice, 385 neurons).

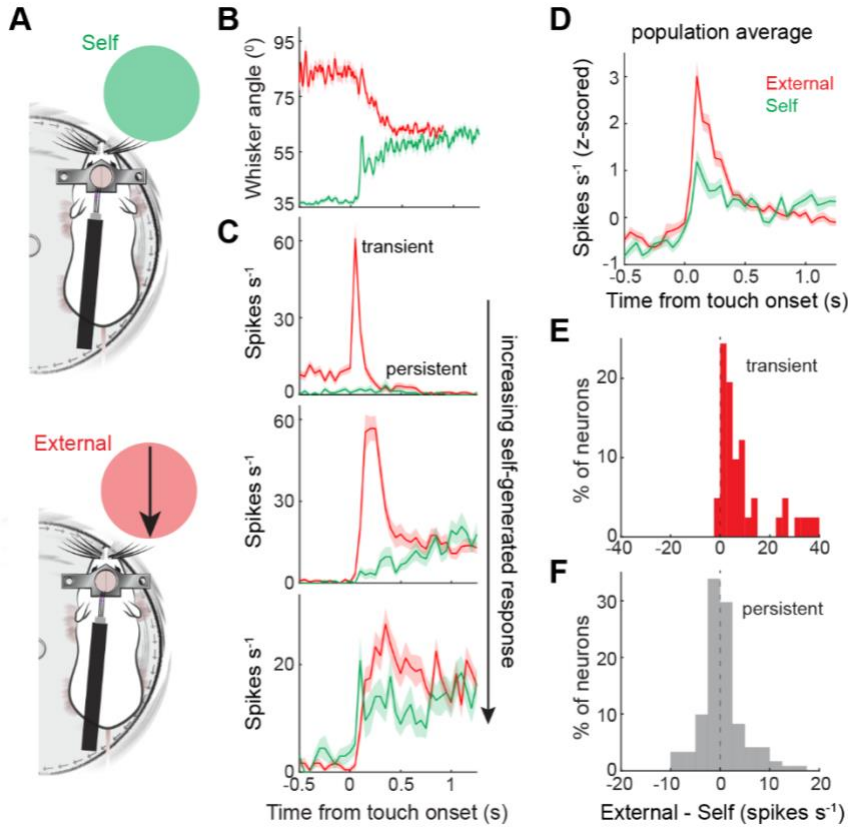

Figure 4. The transient response encodes externally generated changes in whisker space
A) Experimental design comparing GoW from self-motion to GoW from external motion. B) Whisker angle during GoW induced by self- (green) and external motion (red). C) Firing rates of three example neurons aligned to the onset of self- and external GoW. Bottom, a rare neuron with equivalent responses to external and self-GoW. D) Population averaged, z-scored firing rates aligned to the onset of external and self-GoW. E) Firing rates during the transient period were significantly greater from external GoW than from self-GoW ($p = 8e^{-5}$, 2 mice, 41 neurons). F) Firing rates during the persistent period were similar between trials with external and self-GoW ($p = 0.26$, 2 mice, 121 neurons).

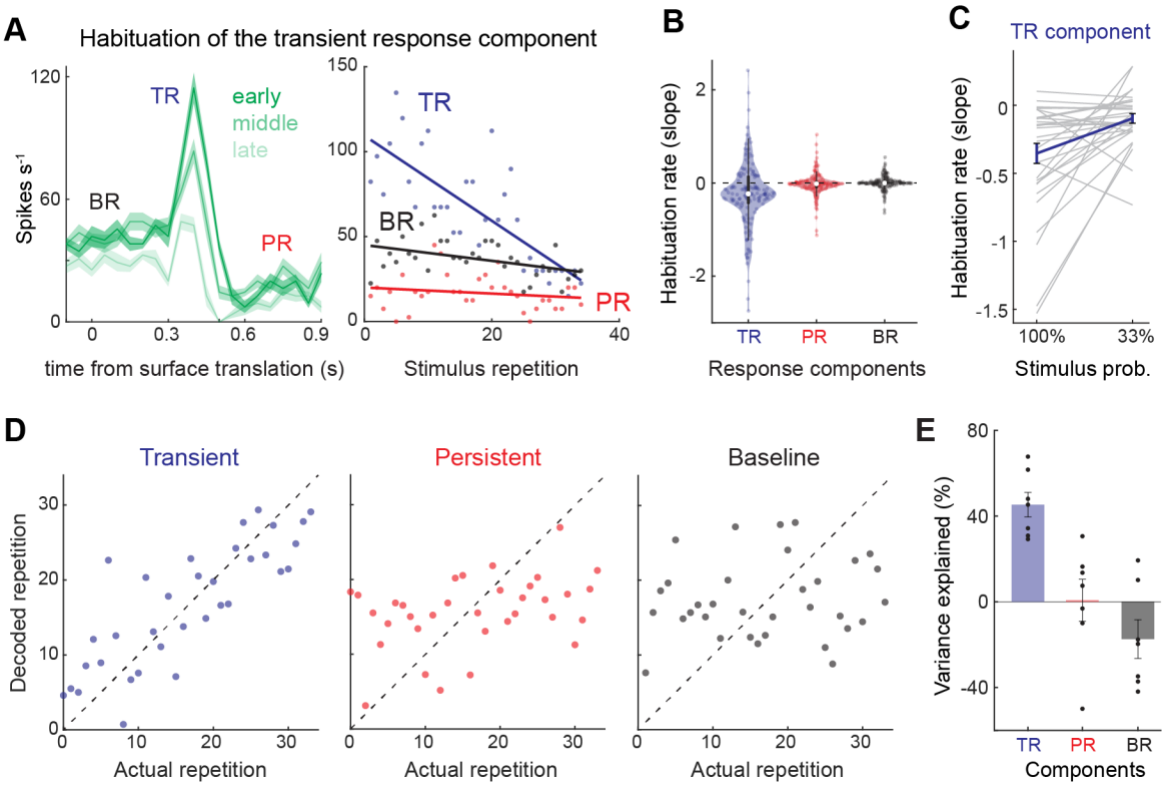

Figure 5. The transient response encodes stimulus novelty
A) Example neuron displaying baseline (BR), transient (TR), and persistent (PR) activity from GoW. The magnitude of each response component as a function of stimulus repetition (early: first third of trials, middle: second third; late: last third). B) Stimulus repetition slopes for neurons with a TR component that were significantly fit by a linear model ($p < 0.05$, t-test). Repetition slopes were calculated separately for the TR, PR, and BR periods (10 mice, 148 neurons). C) The rate of habituation based on stimulus probability (2 mice, 32 neurons with TR during both translations, signrank $p = .0026$). D) Neural decoding of stimulus repetition using each of the response components. Scatter plots comparing the actual stimulus repetition to the neural decoded repetition from a single experiment. E) Decoder performance (variance explained) for the seven mice that accurately predicted stimulus repetition.

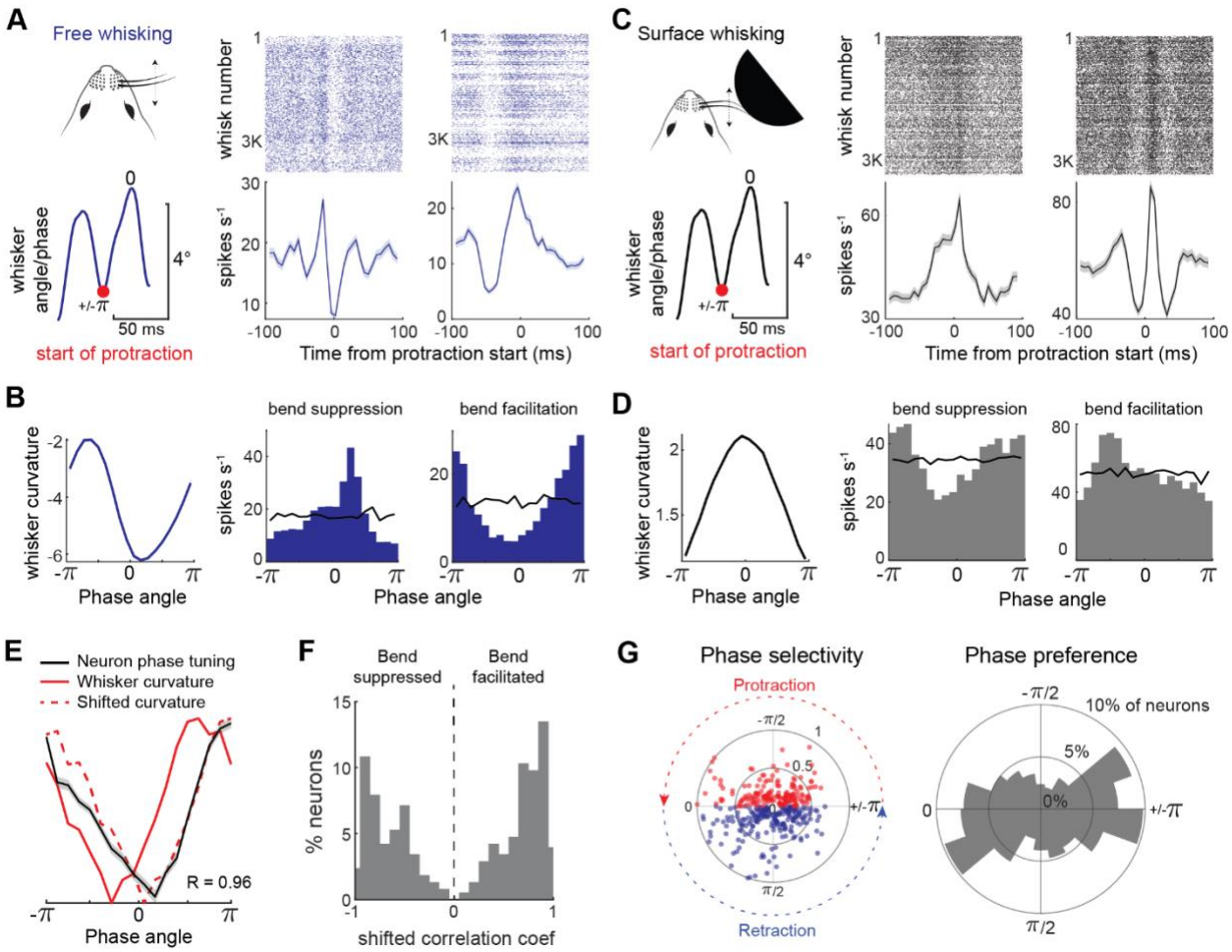

Figure 6. Spike timing is correlated with the rhythm of self-generated tactile features
A) Left, schematic of the relationship between whisker angle and phase. The start of protraction is indicated by the red dot (+/- π). Right, spike rasters and mean firing rates aligned to the onset of whisker protraction during free whisking in air (two neurons). B) Left, whisker curvature as a function of phase (Curvature profile, mean ± s.e.m). Right, phase tuning (STAs) for the two neurons shown in panel A during free whisking in air. The black line illustrates each neuron's chance phase distribution (actual vs. chance: $p = 1e^{-218}$, $p = 3e^{-200}$, chi-squared goodness of fit). C, D) Same as A and B, except during surface whisking ($p = 5e^{-96}$, $p = 8e^{-82}$, chi-squared goodness of fit). E) Phase tuning of an example neuron, its temporally corresponding whisker curvature, and the phase-shifted curvature with the highest correlation coefficient. F) Histogram of the correlation between the phase-shifted curvature profile and the neuronal phase tuning (12 mice, 378 neurons). G) Phase selectivity of neuronal population and a histogram of their phase preferences (12 mice, 378 neurons, 45 ± 3% prefer protraction, 55 ± 3% prefer retraction).

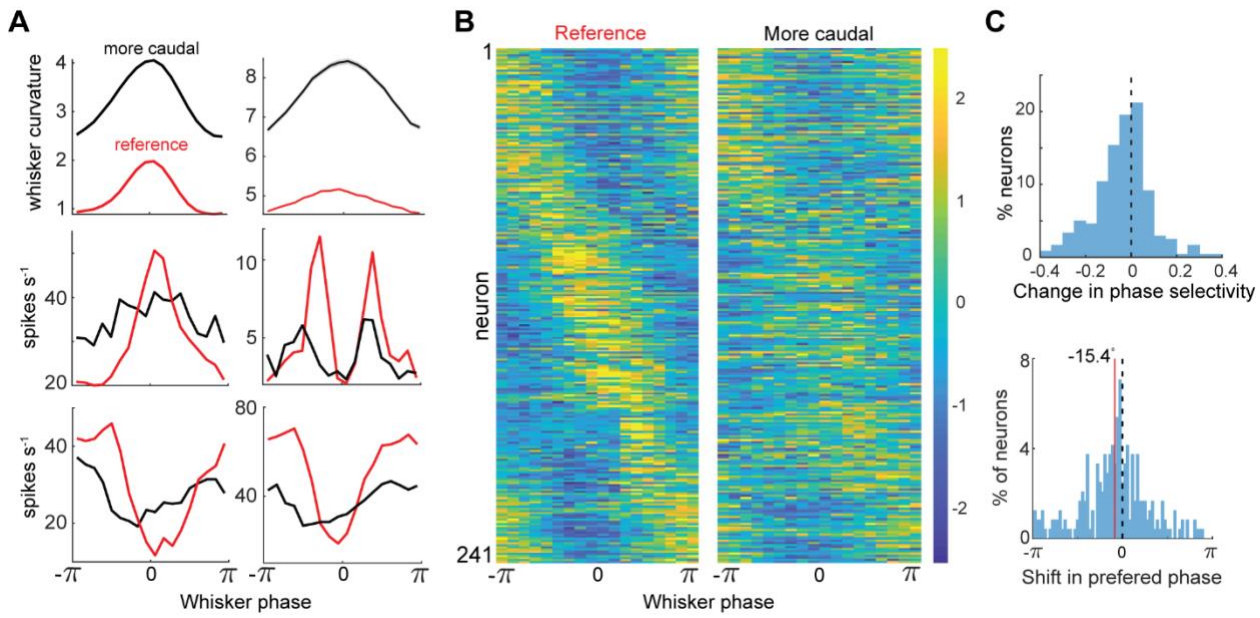

Figure 7. Shifts in spike timing encode self-generated changes in tactile dynamics
A) Curvature profiles (mean ± s.e.m) and their corresponding neuronal phase tuning for two mice (columns) at two surface locations (black vs. red). B) Heatmap of Z-scored phase tuning for neurons at two surface locations (8 mice, 241 neurons). C) Population histograms showing the change in phase selectivity ($p = 5e\text{-}7$, paired t-test, 241 neurons) and the change in phase preference ($p = 0.0056$, paired t-test) from translation into caudal space.

References

1. Munoz, D. P. & Wurtz, R. H. Fixation cells in monkey superior colliculus. II. Reversible activation and deactivation. *J. Neurophysiol.* **70**, 576–589 (1993).

2. Hikosaka, O. & Wurtz, R. H. Modification of saccadic eye movements by GABA-related substances. I. Effect of muscimol and bicuculline in monkey superior colliculus. *J. Neurophysiol.* **53**, 266–291 (1985).

3. Allen, K. M., Lawlor, J., Salles, A. & Moss, C. F. Orienting our view of the superior colliculus: specializations and general functions. *Current Opinion in Neurobiology* **71**, 119–126 (2021).

4. Dräger, U. C. & Hubel, D. H. Topography of visual and somatosensory projections to mouse superior colliculus. *J. Neurophysiol.* **39**, 91–101 (1976).

5. Cang, J., Savier, E., Barchini, J. & Liu, X. Visual Function, Organization, and Development of the Mouse Superior Colliculus. 1–24 (2018). doi:10.1146/annurev-vision-091517

6. Basso, M. A. & May, P. J. Circuits for Action and Cognition: A View from the Superior Colliculus. *Annu. Rev. Vis. Sci.* **3**, 197–226 (2017).

7. Nagy, A., Kruse, W., Rottmann, S., Dannenberg, S. & Hoffmann, K. P. Somatosensory-Motor Neuronal Activity in the Superior Colliculus of the Primate. *Neuron* **52**, 525–534 (2006).

8. Castro-Alamancos, M. A. & Favero, M. Whisker-related afferents in superior colliculus. *J. Neurophysiol.* **115**, 2265–2279 (2016).

9. Bezdudnaya, T. & Castro-Alamancos, M. A. Superior colliculus cells sensitive to active touch and texture during whisking. *J. Neurophysiol.* **106**, 332–346 (2011).

10. Cohen, J. D., Hirata, A. & Castro-Alamancos, M. A. Vibrissa sensation in superior colliculus: wide-field sensitivity and state-dependent cortical feedback. *J. Neurosci.* **28**, 11205–20 (2008).

11. Cohen, J. D. & Castro-Alamancos, M. A. Behavioral State Dependency of Neural Activity and Sensory (Whisker) Responses in Superior Colliculus. *J. Neurophysiol.* **104**, 1661–1672 (2010).

12. Ayaz, A. *et al.* Layer-specific integration of locomotion and sensory information in mouse barrel cortex. *Nat. Commun.* **10**, 1–14 (2019).

13. Jordan, R. & Keller, G. B. Opposing Influence of Top-down and Bottom-up Input on Excitatory Layer 2/3 Neurons in Mouse Primary Visual Cortex. *Neuron* **108**, 1194-1206.e5 (2020).

14. Aronoff, R. *et al.* Long-range connectivity of mouse primary somatosensory barrel cortex. *Eur. J. Neurosci.* **31**, 2221–2233 (2010).

15. Wise, S. P. & Jones, E. G. Somatotopic and columnar organization in the corticotectal projection of the rat somatic sensory cortex. *Brain Res.* **133**, 223–235 (1977).

16. Alloway, K. D., Smith, J. B. & Beauchemin, K. J. Quantitative analysis of the bilateral brainstem projections from the whisker and forepaw regions in rat primary motor cortex.

J. Comp. Neurol. **518**, 4546–4566 (2010).

17. Singla, S., Dempsey, C., Warren, R., Enikolopov, A. G. & Sawtell, N. B. A cerebellum-like circuit in the auditory system cancels responses to self-generated sounds. *Nat. Neurosci. 2017 207* **20**, 943–950 (2017).

18. Shadmehr, R., Smith, M. A. & Krakauer, J. W. Error correction, sensory prediction, and adaptation in motor control. *Annual Review of Neuroscience* **33**, 89–108 (2010).

19. Kilteni, K. & Henrik Ehrsson, H. Functional Connectivity between the Cerebellum and Somatosensory Areas Implements the Attenuation of Self-Generated Touch. *J. Neurosci.* **40**, 894–906 (2020).

20. Anderson, S. R. *et al.* An Internal Model Architecture for Novelty Detection: Implications for Cerebellar and Collicular Roles in Sensory Processing. *PLoS One* **7**, e44560 (2012).

21. Kojima, Y. & Soetedjo, R. Elimination of the error signal in the superior colliculus impairs saccade motor learning. *Proc. Natl. Acad. Sci. U. S. A.* **115**, E8987–E8995 (2018).

22. Lee, J. & Sabatini, B. L. Striatal indirect pathway mediates exploration via collicular competition. *Nat. 2021* 1–5 (2021). doi:10.1038/s41586-021-04055-4

23. Jiang, H., Stein, B. E. & McHaffie, J. G. Opposing basal ganglia processes shape midbrain visuomotor activity bilaterally. *Nature* **423**, 982–986 (2003).

24. Liu, P. & Basso, M. A. Substantia nigra stimulation influences monkey superior colliculus neuronal activity bilaterally. *J. Neurophysiol.* **100**, 1098–1112 (2008).

25. Kaneda, K., Isa, K., Yanagawa, Y. & Isa, T. Nigral inhibition of GABAergic neurons in mouse superior colliculus. *J. Neurosci.* **28**, 11071–11078 (2008).

26. Lee, J., Wang, W. & Sabatini, B. L. Anatomically segregated basal ganglia pathways allow parallel behavioral modulation. *Nat. Neurosci.* **23**, 1388–1398 (2020).

27. Mcelvain, L. E. *et al.* Specific populations of basal ganglia output neurons target distinct brain stem areas while collateralizing throughout the diencephalon In brief. *Neuron* **109**, 1–18 (2021).

28. Villalobos, C. A., Correspondence, M. A. B. & Basso, M. A. Optogenetic activation of the inhibitory nigro-collicular circuit evokes contralateral orienting movements in mice. *Cell Rep.* **39**, 110699 (2022).

29. Lee, K. H., Tran, A., Turan, Z. & Meister, M. The sifting of visual information in the superior colliculus. *Elife* **9**, (2020).

30. Basso, M. A. & Wurtz, R. H. Modulation of neuronal activity by target uncertainty. *Nat. 1997 3896646* **389**, 66–69 (1997).

31. Griggs, W. S., Amita, H., Gopal, A. & Hikosaka, O. Visual neurons in the superior colliculus discriminate many objects by their historical values. *Front. Neurosci.* **12**, 396 (2018).

32. Basso, M. A. & Wurtz, R. H. Modulation of Neuronal Activity in Superior Colliculus by Changes in Target Probability. *J. Neurosci.* **18**, 7519–7534 (1998).

33. Zhang, B. *et al.* Transforming absolute value to categorical choice in primate superior colliculus during value-based decision making. *Nat. Commun. 2021 121* **12**, 1–14 (2021).

34. Boehnke, S. E. *et al.* Visual adaptation and novelty responses in the superior colliculus. *Eur. J. Neurosci.* **34**, 766–779 (2011).

35. Lee, K. H., Tran, A., Turan, Z. & Meister, M. The sifting of visual information in the superior colliculus. (2016).

36. Dr;, U. C., Ger, ;, David, A. & Hubel, H. Responses to visual stimulation and relationship between visual, auditory, and somatosensory inputs in mouse superior colliculus. *J. Neurophysiol.* **38**, 690–713 (1975).

37. Cynader, M. & Berman, N. Receptive-field organization of monkey superior colliculus. *J. Neurophysiol.* **35**, 187–201 (1972).

38. Wallach, A., Bagdasarian, K. & Ahissar, E. On-going computation of whisking phase by mechanoreceptors. *Nat. Neurosci. 2016 193* **19**, 487–493 (2016).

39. Isett, B. R. & Feldman, D. E. Cortical Coding of Whisking Phase during Surface Whisking. *Curr. Biol.* 1–10 (2020). doi:10.1016/j.cub.2020.05.064

40. Ebert, C., Bagdasarian, K., Haidarliu, S., Ahissar, E. & Wallach, A. Interactions of Whisking and Touch Signals in the Rat Brainstem. *J. Neurosci.* **41**, 4826–4839 (2021).

41. Severson, K. S. *et al.* Active Touch and Self-Motion Encoding by Merkel Cell-Associated Afferents. *Neuron* **94**, 666-676.e9 (2017).

42. Cheung, J., Maire, P., Kim, J., Sy, J. & Hires, S. A. The Sensorimotor Basis of Whisker-Guided Anteroposterior Object Localization in Head-Fixed Mice. *Curr. Biol.* **29**, 3029-3040.e4 (2019).

43. Szwed, M., Bagdasarian, K. & Ahissar, E. Encoding of vibrissal active touch. *Neuron* **40**, 621–630 (2003).

44. Knutsen, P. M., Pietr, M. & Ahissar, E. Haptic object localization in the vibrissal system: behavior and performance. *J. Neurosci.* **26**, 8451–64 (2006).

45. Mathis, A. *et al.* DeepLabCut: markerless pose estimation of user-defined body parts with deep learning. *Nat. Neurosci.* **21**, 1281–1289 (2018).

46. Pachitariu, M., Steinmetz, N., Kadir, S., Carandini, M. & D., H. K. Kilosort: realtime spike-sorting for extracellular electrophysiology with hundreds of channels. *bioRxiv* 061481 (2016). doi:10.1101/061481

47. Meyers, E. The neural decoding toolbox. *Front. Neuroinform.* **7**, 8 (2013).

48. Berens, P. CircStat: A MATLAB Toolbox for Circular Statistics. *J. Stat. Softw.* **31**, 1–21 (2009).